He *et al. Carbon Research* (2023) 2:18
https://doi.org/10.1007/s44246-023-00050-8

Carbon Research

ORIGINAL ARTICLE

Open Access

Unraveling the role of natural and pyrogenic dissolved organic matter in photodegradation of biodegradable microplastics in freshwater

Jiehong He[1,2†], Weiwei Ma[1,2†], Lanfang Han[1,2*], Liying Chen[1,2], Elvis Genbo Xu[3], Baoshan Xing[4] and Zhifeng Yang[1,2]

Abstract

Biodegradable plastic is often perceived as a possible solution for microplastic (MP) pollution. Photodegradation is an important transformation pathway of biodegradable MPs in aquatic environments. However, the influence mechanisms of dissolved organic matter (DOM) from different sources on photodegradation of biodegradable MPs are poorly understood. This study explored the role of naturally and pyrogenically sourced DOM in the photodegradation of polylactic acid (PLA) MPs. The aromatics of natural DOM (NDOM) were higher than those of biochar-sourced DOM (BDOM) and showed a stronger improvement in PLA-MPs degradation, as evidenced by particle size reduction, crystallinity increase and polymerization decrease, breakage of surface morphology, and increase in oxygen-containing functional groups on MPs' surface (O/C increase: 65.1% for NDOM; 34.9% for BDOM). Reactive oxygen species analysis showed that the excited triplet states of DOM ($^3DOM^*$) generated by NDOM produced more •OH and $^1O_2$ than that of BDOM, accelerating PLA-MPs photodegradation. Such photodegradation processes were further enhanced through the sorption of DOM by PLA-MPs, in which non-aromatic components were preferentially sorbed, causing the enrichment of aromatics in the solution, leading to more $^3DOM^*$ formation. This study improves the understanding of the migration and transformation of biodegradable MPs with the presence of DOM.

Highlights

1. Natural-sourced DOM had more aromatics than pyrogenic-sourced one, which strongly improved PLA-MPs photodegradation.
2. •OH species played a dominant role in PLA-MPs photodegradation.
3. The preferential sorption of non-aromatics by PLA-MPs favored photodegradation.

Keywords Microplastics, Photodegradation, Aromatic component, Reactive oxygen species

† Jiehong He and Weiwei Ma are contributed equally to this work.

Handling editor: Bo Pan.

*Correspondence:
Lanfang Han
hanlanfang@gdut.edu.cn
Full list of author information is available at the end of the article

Graphical Abstract

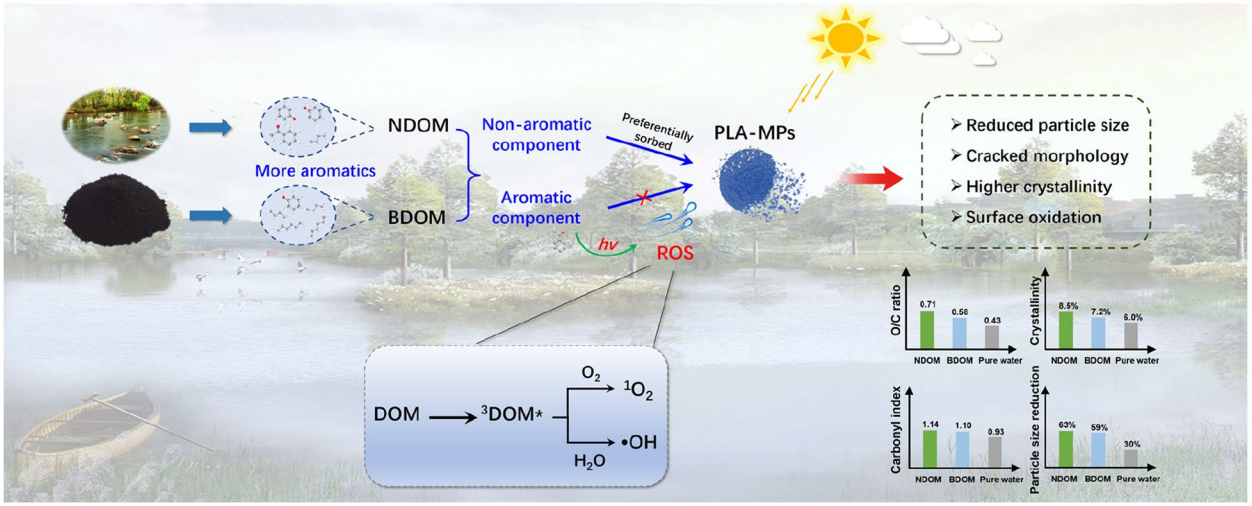

1 Introduction

It has been estimated that about 12 billion metric tons of plastic wastes will be released into the environment by 2050 year. Most of the plastic wastes could be degraded into plastics with sizes smaller than 5 mm (known as microplastics; MPs) under light irradiation, wind erosion, water abrasion, and other environmental processes (Lin et al. 2022). So far, MPs have been found in different ecosystems (e.g., freshwaters (Li et al. 2018a), oceans (Everaert et al. 2020), and soils (Xiang et al. 2022)), and have raised concerns about their long-term environmental impacts, which are related to their non-biodegradability, persistence in nature and toxic effects on organisms (Kim et al. 2020; Wang et al. 2021). Thus, to alleviate MPs pollution, conventional non-biodegradable plastics (e.g., polyethylene (PE), polypropylene (PP), polystyrene (PS)) have been replaced with biodegradable plastics (e.g., polylactic acid (PLA), poly(ε-caprolactone) (PCL)) in the market (Qin et al. 2021; Wei et al. 2021). These biodegradable plastics could be completely transformed into environmentally benign substances in controlled biological transformation environments (e.g., industrial composting sites) (Filiciotto and Rothenberg 2021; Gioia et al. 2021). However, since it is difficult for the natural environment to provide such conditions, MPs may also be generated from biodegradable plastics and remain for a long period of time like conventional plastics (Liao and Chen 2021). Moreover, because biodegradable plastics are more easily degraded, they might produce more MPs over the same period in the environment (Liao and Chen 2021). As recently reported by Wei et al. (2022), the number of formed MPs from the biodegradation of 0.1 g PCL could be as high as one million. Consequently, the fate and transformation of biodegradable MPs urgently need to be clarified.

Both conventional and biodegradable MPs can undergo biotic and abiotic environmental processes (Ali et al. 2021), and photodegradation induced by ultraviolet (UV) light irradiation has been considered an important transformation pathway of MPs in the aquatic environment (Chen et al. 2019; Shi et al. 2021). In recent years, extensive studies have explored the photodegradation process of MPs under aqueous conditions, and have confirmed that the reactive oxygen species (ROS), such as hydroxyl radical (•OH), singlet oxygen ($^1O_2$), and superoxide anion radical ($•O_2^-$), enabled the acceleration of this process (Zhu et al. 2020; Zhu et al. 2019). Also, focusing on conventional non-biodegradable plastics like PE, PP, and PS, researchers have found that different types of MPs, due to the differences in polymer compositions and properties, have different photodegradation mechanisms (Liu et al. 2022). However, the photodegradation mechanisms of biodegradable MPs remain unclear, particularly under environmentally realistic conditions.

Dissolved organic matter (DOM) is ubiquitous in freshwater with the concentration ranging from a few to tens of mg/L. For example, the DOM concentration ranged from 4.2 to 31.3 mg/L in fresh and saline lakes of Northern China (Wen et al. 2018), and was 10.3–18.3 mg/L in Heilongjiang watershed (Shi et al. 2016). The DOM amount in the overlying water of Lake Taihu was

2.9–11.8 mg/L and mainly contained humic acid-type species and tyrosine-like components (Gao et al. 2017). Sunlight-irradiated DOM can lead to the formation of ROS, such as excited triplet states of DOM ($^3DOM^*$), •OH, and $^1O_2$, thereby accelerating the photodegradation of organic pollutants (Zhang et al. 2014). The formed $^3DOM^*$ can react with various pollutants such as herbicides (Canonica and Silvio 2007) and antibiotics (Li et al. 2015). However, DOM may also inhibit the photodegradation of organic pollutants through scavenging ROS and shielding sunlight (Niu et al. 2018). The specific role of DOM in the photodegradation of a specific organic pollutant was dependent upon the sources of DOM (Wang et al. 2019). It was reported that the DOM in freshwater could be sourced from natural processes (e.g., microbial metabolism) and the runoff of surrounding soil (Luo et al. 2021), which can significantly affect the photodegradation of MPs (Wang et al. 2020). Pyrogenic carbon is a substantial portion of soil organic carbon. Currently, the application of pyrogenic carbon in the form of biochar plays an essential role in the global carbon budget (Yang et al. 2022). DOM released from biochar (BDOM) could be readily mobilized from soils by infiltration and surface runoff and becomes one of the main forms of pyrogenic carbon in freshwater. Wagner et al. (2018) have estimated that 10% of DOM in rivers is in the form of dissolved pyrogenic carbon (pyDOM). Due to the diverse compositions of DOM from various sources, the corresponding $^3DOM^*$ has different excited-state potentials (Mcneill and Canonica 2016; Ryan et al. 2011). Recently, Qiu et al. (2022) have studied the interaction between DOM and PS MPs and proved the crucial role of ROS derived from DOM in PS MPs photoaging. Luo et al. (2022) demonstrated that the interaction between PP MPs and humic acid was associated with aromatic structures, leading to elevated surface oxygen-containing functional groups. Additionally, Ding et al. (2022a) explored the binding of different DOMs to PS MPs and found that the combination of MPs was determined by the structure of DOM, with the oxygen-containing functional groups on the surface of PS MPs being the preferred binding sites. Thus, the interaction of DOM and MPs is associated with DOM structure. On the basis of the different compositions and structures of natural DOM (NDOM) and BDOM (Hiemstra et al. 2013), we hypothesize that NDOM and BDOM have different effects on the photodegradation of biodegradable MPs due to the differences in the composition, free radical formation, etc. However, most of the previous studies have focused on traditional MPs (e.g., PS and PP). There is a shortage of comparative information on the transformation of biodegradable MPs mediated by NDOM and BDOM. The relationship between the compositions of DOM from different sources in freshwater and the photodegradation of biodegradable MPs remains to be revealed. This knowledge gap hinders our understanding of the fate and impact of MPs in freshwater with the presence of diverse DOM.

In this study, we targeted polylactic acid (PLA), one of the most common biodegradable polymers. The main objective was to elucidate the regulating mechanisms of NDOM and BDOM on the photodegradation of PLA-MPs in aqueous solutions under UV light irradiation through exploring the properties of PLA-MPs (e.g., particle size, surface morphology and oxygen-containing functional groups), the composition variations of DOMs and ROS generation. The photodegradation pathways of PLA-MPs and mediating mechanisms of NDOM and BDOM were revealed. The results would advance the understanding of the photochemical transformation of biodegradable MPs in the environmental relevant conditions.

2 Materials and methods

2.1 Preparation of PLA-MPs, BDOM, and NDOM

PLA-MP powder was purchased from Guangzhou Huayu Environmental Technology, Inc. (Guangzhou, China) and washed with ultrapure water several times before use. Suwanee River natural organic matter was purchased from the International Humic Substance Society (IHSS) and used as NDOM. BDOM was extracted from biochar produced at medium (450 °C) temperature because preliminary experiments showed that biochar at relatively high temperature (e.g., 600 °C) was greatly graphitized and produced insufficient amounts of BDOM for further experimental use. And for biochar at comparatively low temperatures (e.g., 300 °C), DOM was insufficiently pyrolyzed (Sun et al. 2016). More details were provided in the supplementary information.

2.2 Photodegradation of PLA-MPs

The photodegradation of PLA-MPs was performed in a PCX-50C Discover multi-channel photocatalytic reactor (Beijing Perfect Light Technology Co., Ltd., China) equipped with nine 365 nm LED (5 W) as the light source for each channel since UV radiation is considered one of the most important factors in material photodegradation in natural environment (Ding et al. 2022b; Mao et al. 2020; Wang et al. 2022). Before reaction, the initial concentration of BDOM and NDOM was determined by a total organic carbon analyzer (Shimadzu TOC-L, Japan) and adjusted to 10 mg/L with 30 mL ultrapure water, which was close to the average concentration in freshwater (Lyu et al. 2021) and met the surface water quality standard of class III in GB3838-2002, China. Then, the BDOM and NDOM solutions were transferred to a 50 mL glass vial, respectively, and 30 mg PLA-MPs were

added. The MPs concentration in the experiment was determined according to the previous studies (Chen et al. 2020; Ding et al. 2022b). The suspension was sealed and sonicated to ensure good dispersion. After that, the light was turned on to initiate the reaction. The reaction temperature was controlled at 25 °C with a circulating water bath, and the solution was stirred to ensure well mixing of MPs with DOM solution. The reaction solution and photodegraded PLA-MPs were separated with a nylon filter membrane (0.45 μm) after different irradiation time points (0, 1, 2, 3, 4, 5, 6, and 7 d). The photodegraded PLA-MPs were then washed using ultrapure water to remove the residue (e.g., DOM) on the surface, which was freeze-dried and stored in dark. Also, the photodegradation of PLA-MPs in pure water (without BDOM or NDOM) was performed for comparison, and PLA-MPs in dark were conducted as the control group. The light shielding effect of DOM and quenching effect on the PLA-MPs photodegradation were evaluated. The details were shown in the supplementary information.

2.3 Characterization of PLA-MPs

The surface morphology, particle size, functional group, crystallinity, surface composition, degree of polymerization and molecular weight of the original and photodegraded PLA-MPs were determined by field emission scanning electronic micrograph (FESEM, Hitachi SU8220, Japan), optical microscope (Olympus CKX53, Japan), X-ray photoelectron spectroscopy (XPS, Thermo Scientific K-Alpha Nexsa using Al K Alpha radiation, America), X-ray diffraction (XRD, Rigaku Ultima VI, Japan) patterns, Fourier Transform Infrared Spectrometer (FTIR, Shimadzu IRTracer-100, Japan) and ^{1}H Nuclear Magnetic Resonance Spectroscopy (^{1}H-NMR, Bruker Avance NEO 600, America), respectively, as detailed in the supplementary information. During the process of PLA-MPs photoaging, the reduction of average particle size was calculated based on the ratio of the difference value of pristine and aged PLA-MPs to the particle size of pristine PLA-MPs. The carbonyl index (CI) was calculated based on the ratio of the area of the carbonyl absorption band at 1750 cm^{-1} to the area of the reference absorption band at 1450 cm^{-1} (assigned to C-H stretching in methyl groups of PLA-MPs in FTIR), as detailed in supplemental information.

2.4 Characterization of BDOM and NDOM

The alterations of BDOM and NDOM structures, and TOC concentrations were determined by fluorescence excitation-emission matrix (EEM) spectra (Shimadzu RF-6000, Japan), Electrospray Ionization-Fourier Transform-Ion Cyclotron Resonance-Mass Spectrometry (ESI-FT-ICR-MS, Bruker SolariX**,** America), TOC analyzer (Shimadzu TOC-L, Japan), and UV–vis absorption spectra (Shimadzu UV-2700, Japan), respectively, as detailed in the supplementary information. The $SUVA_{254}$ (Specific ultraviolet absorbance in 254 nm, a proxy for aromaticity of DOM) was determined by normalizing the specific ultraviolet absorbance at 254 nm of UV–vis spectra to TOC concentration.

2.5 Sorption of BDOM and NDOM on PLA-MPs and identification of free radicals

The sorption of NDOM and BDOM on PLA-MPs was conducted in dark, and the changes in compositions of NDOM and BDOM remaining in solution by sorption were determined with UV–vis, EEM, and FTIR, as detailed in the supplementary information. The formation of $^{1}O_2$, •OH, and carbon-centered radical during PLA-MPs photodegradation was analyzed by Electron Paramagnetic Resonance (EPR) spectrometer (Bruker EMXplus, Germany), and qualification of free radicals was conducted by adding different trapping agents, as detailed in the supplementary information.

2.6 Statistical analysis

Statistical analysis was conducted using one-way analysis of variance (ANOVA) and *P*-values < 0.05 were considered significant. IBM Statistical Products and Services Solutions (SPSS 23.0) software was adopted to analyze particle size reduction, crystallinity, TOC, $SUVA_{254}$. NS presented no significance, while * (probability value, $p < 0.05$) and ** ($p < 0.01$) were regarded as statistically significant differences compared with the control group. In addition, all correlation experiments were conducted in triplicate, and the experiment results are expressed as the mean values ± standard deviation (SD).

3 Results and discussion

3.1 Comparisons of structures of BDOM and NDOM

As shown in Fig. 1, the EEM spectra of each DOM sample maintained the consistent excitation and emission wavelength boundaries, which was divided into five regions (I-V) corresponding to tyrosine-, tryptophan-, fulvic acid-, soluble microbial byproduct- and humic acid-like (HA) fraction, respectively. Differences in the relative abundance of these components were noted for BDOM and NDOM. Humic acid-like fraction (Region V) was found as the main component (> 60.0%) and was more abundant in NDOM (73.4%) compared with that in BDOM (63.9%). By contrast, the relative abundance of fulvic acid-, microbial by-product- and tryptophan protein-like fraction in BDOM were slightly higher than in NDOM (Fig. 1j). Since humic acid-like fraction generally showed higher aromatics relative to other components (Chen et al. 2003).

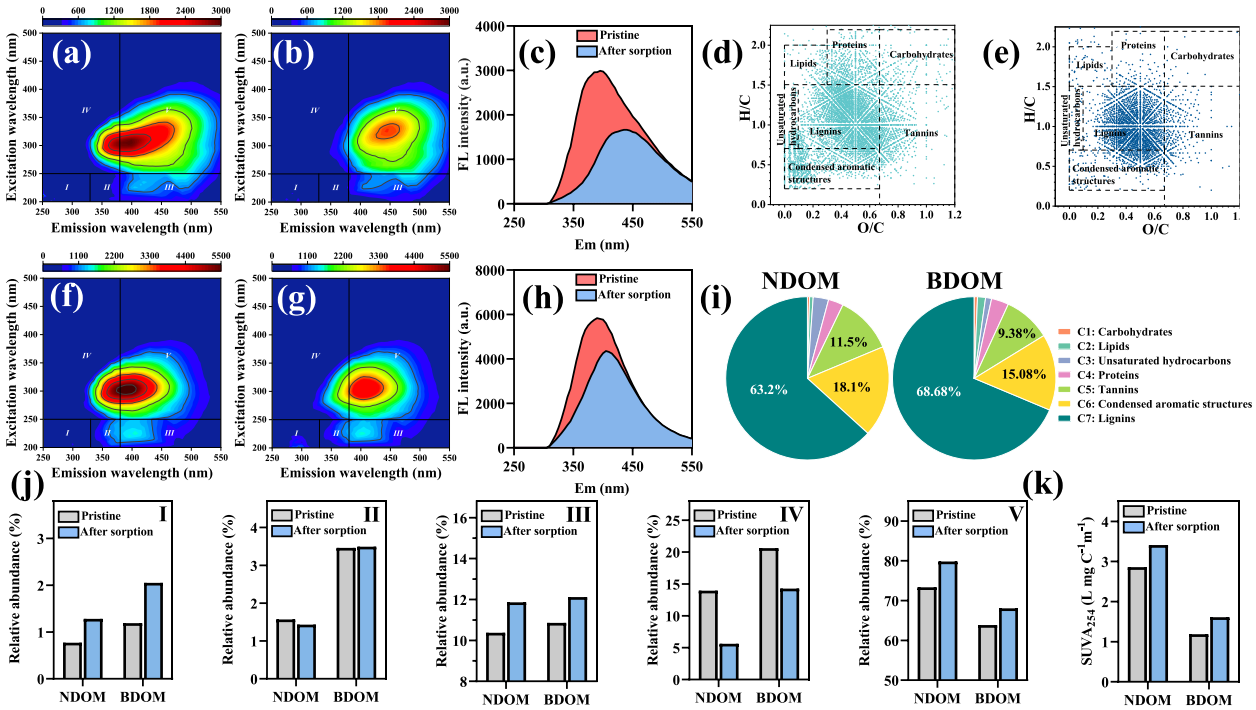

Fig. 1 The excitation-emission matrix spectrums of natural dissolved organic matter (NDOM) before (**a**) and after (**b**) 72 h sorption and their corresponding fluorescence intensity (**c**); Van Krevelen diagrams of NDOM (**d**) and biochar-derived dissolved organic matter (BDOM) (**e**); the excitation-emission matrix spectrums of BDOM before (**f**) and after (**g**) 72 h sorption and their corresponding fluorescence intensity (**h**); the relative abundance of different compounds in NDOM and BDOM (**i**); regional integration of excitation-emission matrix spectroscopies related to different organic carbon components (**j**) (I: tyrosine protein-like species; II: tryptophan protein-like species; III: fulvic acid-like species; IV: microbial by-product analogues; V: humic acid-like species) and the $SUVA_{254}$ (Specific ultraviolet absorbance of 254 nm in UV–vis spectrum) (**k**) of NDOM and BDOM remaining in solutions before and after 72 h sorption. Note that Fig. 1c and h was obtained with the excitation wavelength of 305 nm, and the peak area in the red region was covering the blue region

These results suggested more aromatic components of NDOM than BDOM, which was evidenced by $SUVA_{254}$ data. The value of $SUVA_{254}$ in NDOM (2.9) was obviously higher than BODM (1.2) (Fig. 1k). The ESI-FT-ICR-MS analysis was also performed to compare the molecular compositions of NDOM and BDOM (Lv et al. 2016). Based on the values of O/C and H/C, the Van Krevelen diagrams were constructed and the molecular composition was classified into carbohydrate-, unsaturated hydrocarbon-, protein-, tannin-, condensed aromatic structure-, and lignin-like components. The BDOM and NDOM were mainly composed of lignin-, condensed aromatic structure- and tannin-like species (Fig. 1d and e). Consistent with UV–vis and EEM data, the aromatic index (AI), as a proxy for the aromaticity of molecular (Miao et al. 2020), was about 1.1 times higher in NDOM (1.04) than in BDOM (0.43) (Table S1). In addition, the relative abundance of condensed aromatic-like fraction was relatively higher in NDOM (15.1% in BDOM and 18.1% in NDOM) (Fig. 1i). Commonly, BDOM was considered to have more (condensed) aromatics than NDOM due to the aromatic nature of biochar (Jaffé et al. 2013). In contrast, our findings manifested that the aromatic content of BDOM was not necessarily higher than that of NDOM. This was well consistent with the recent findings of Goranov et al. (2020) that the aryl group in pyrogenic-sourced DOM was not stable and the alkyl and O-alkyl groups were more likely to be produced, and pyrogenic-sourced DOM from leachates of higher temperature biochar (525 and 650 °C) transformed predominantly into smaller aliphatic compounds.

3.2 Altered characteristics of PLA-MPs during photodegradation process

The particle size of MPs, as one indicator of photodegradation extent, was determined at different time points (Fig. 2a). Under the dark condition, no obvious reduction in particle size of PLA-MPs was observed. In the photodegradation at pure water, the particle size of PLA-MPs decreased by around 30.4% after 3 d of irradiation. In the presence of NDOM and BDOM, the particle size reduction increased to 62.8% and 59.1%, respectively. Further, the first-order reaction kinetics were used to simulate the

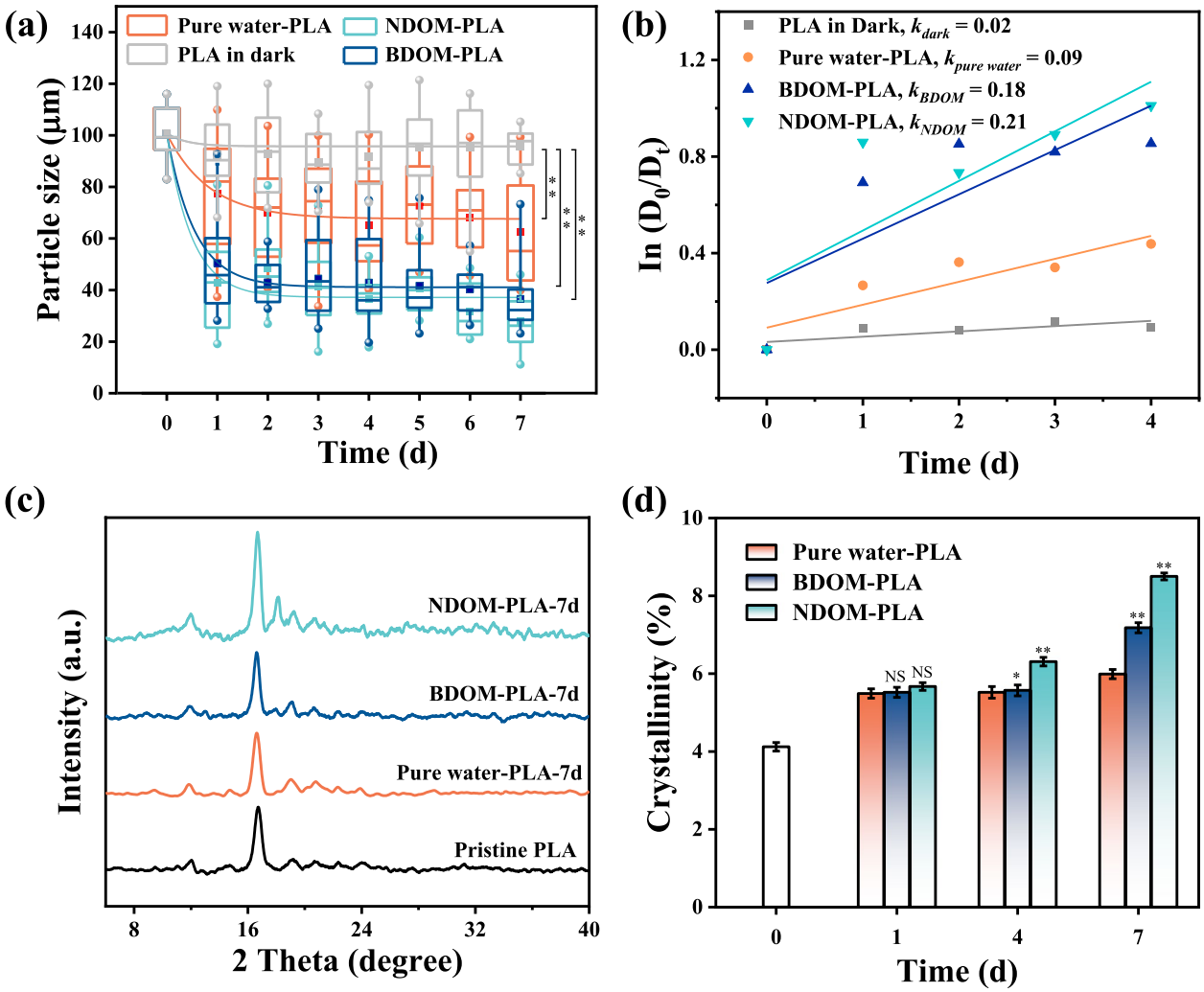

Fig. 2 The particle size reduction (**a**) and the corresponding first-order kinetic fit of the reaction (**b**), X-Ray diffraction patterns (**c**) of polylactic acid (PLA) microplastics (MPs) with irradiation in pure water, natural dissolved organic matter (NDOM) and biochar-derived dissolved organic matter (BDOM) solution, and their corresponding crystallinity (**d**). Note that dark control was conducted as a comparison. The reaction rate (*k*) was based on the rapid reduction of particle size in the first 4 d in Fig. 2a. "D_0" was the pristine particle size of PLA-MPs and "D_t" was the average particle size of aged PLA-MPs after t d. NS presented no significance, while * ($p < 0.05$) and ** ($p < 0.01$) were regarded as statistically significant differences compared with control group (Pure water-PLA)

particle size change. Since all samples were essentially stable at the later period, the reaction rates were calculated for the first 4 days and were obtained in Fig. 2b. *k* value lied in the order of k_{NDOM} (0.21) > k_{BDOM} (0.18) > $k_{\mathrm{pure\ water}}$ (0.09). These results suggested that the reduction degree and rate of particle sizes of PLA-MPs were promoted in the presence of either NDOM or BDOM compared to pure water, and the promotion was slightly stronger for NDOM. This was also supported by the analysis of the surface morphology of PLA-MPs under different conditions. The pristine PLA-MPs displayed a smooth and flat surface, and in the dark control, no obvious change was found (Fig. 3b). However, accompanied by the decreased particle size, plentiful cracks and holes were formed on the outer layer after 7 d of UV irradiation in pure water (Fig. 3c). Additionally, more holes and defects were observed in the presence of DOM (Fig. 3d and e), especially NDOM. Also, similar to the FESEM result, compared to the pure water, the accelerated effect of both NDOM and BDOM on photodegradation of PLA-MPs was also indicated by the increase of the TOC in solution (Fig. S1), which was ascribed to the release of the organic compounds from photodegraded PLA-MPs. The downtrend of TOC in the late period for all samples might be ascribed to mineralization or the sorption of organic matter by photodegraded PLA-MPs (Liu et al. 2022).

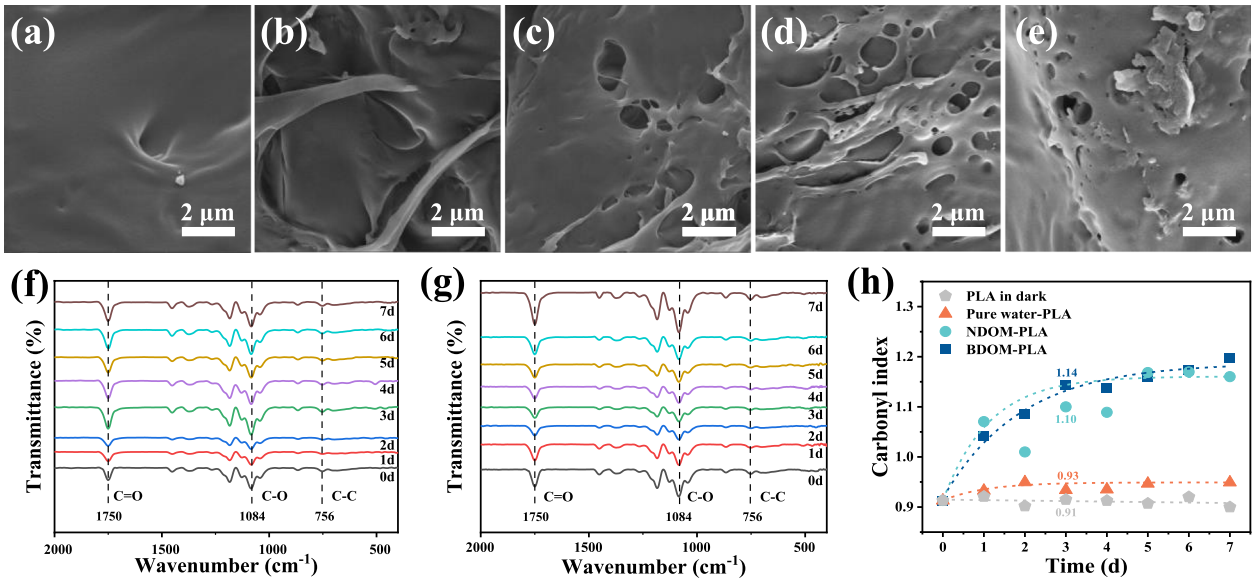

Fig. 3 Scanning electron microscope images (a-e) of pristine polylactic acid (PLA) microplastics (MPs) (**a**), dark control (**b**), photodegraded PLA-MPs in pure water (**c**), natural dissolved organic matter (NDOM) (**d**) and biochar-derived dissolved organic matter (BDOM) (**e**) solution after different time irradiation; Fourier transform infrared spectra of PLA-MPs during irradiation in NDOM (**f**) and BDOM (**g**) solution, and their corresponding carbonyl index variation with irradiation time (**h**)

The alterations in crystallinity of PLA-MPs were demonstrated from the XRD spectra of PLA-MPs after 1 d, 4 d, and 7 d irradiation in pure water, NDOM and BDOM treatments (Fig. S2). PLA is known to crystallize in three different crystal forms: α, β, and γ (Simmons et al. 2019), in which α was the most common structure with two distinct phases including α (stable) and α′ (disordered) (Lv et al. 2018). All samples exhibited diffraction peaks at 16.5° and 19.0°, corresponding to the (110)/(200) and (203) reflection of the disordered α′ crystals, respectively (Buzarovska et al. 2015). As the photodegradation time prolonged, several diffraction peaks (e.g., 18.9°, and 22.2°) were found in photodegraded PLA, especially for the samples treated with NDOM and BDOM, indicating the increase in crystallinity (Fig. 2c). Additionally, the photodegraded PLA-MPs with NDOM treatment exhibited higher intensity of the peak at 16.5° compared to BDOM and pure water, indicating higher crystallinity. The degree of crystallinity of the photodegraded PLA-MPs was quantified by the integration of the crystalline peak areas from XRD diffractograms (Fig. 2d). The pristine PLA-MPs showed crystallinity of 4.1%, which was caused by the chain conformation and packing between the disordered and ordered forms (Kalish et al. 2011). As the irradiation time prolonged, the crystallinity of PLA-MPs gradually increased. After 7 d, the crystallinity of PLA-MPs declined in the order of NDOM (8.5%) > BDOM (7.2%) > pure water (6.0%). The change in crystallinity of PLA-MPs could be explained by the preferential photo-oxidation and weathering of the amorphous components (Miranda et al. 2021). In addition, the chain scission caused by photo-oxidation could result in more amorphous chains recombined and further crystallized by chemi-crystallization, resulting in increased crystallinity (Sang et al. 2020). Therefore, the addition of BDOM or NDOM revealed a promoting effect on the photodegradation of PLA-MPs, leading to the improvement of crystallinity, and this process was more significant with NDOM treatment.

With the photo-oxidation on the surface of PLA-MPs, the distribution of functional groups was dissimilarly altered under different reaction conditions. As seen in Fig. 3f-g, pristine PLA-MPs presented the distinct band at 1750 and 1185 cm^{-1}, corresponding to C=O stretching and C–O–C stretching, respectively (Yang et al. 2008). The band at 1450 cm^{-1} was due to C-H stretching in methyl groups (Paragkumar et al. 2006). The faint peaks at 1265 cm^{-1} (δ-C-H + ν-C–O–C) and 1210 cm^{-1} (vas-C–O–C + CH_3) were also noticed as the typical pattern of PLA-MPs (Leroy et al. 2017). The bands at 1044, 1084 and 1128 cm^{-1} were attributed to C-O stretching vibrations of PLA-MPs (Pamuła et al. 2001). As the irradiation time was prolonged, the relative intensity of the carbonyl band at 1750 cm^{-1} of all the samples increased, indicating the accumulation of oxygen-related functional groups on the surface of PLA-MPs during photodegradation. Further, the carbonyl index (CI) value was calculated to quantify the photodegradation degree

of PLA-MPs. As displayed in Fig. 3h, CI value of all the PLA-MPs reached an equilibrium state after around 3 d irradiation, which might be attributed to the limited diffusion ability of oxygen or free radicals to the inner layer of MPs during the photodegradation process (ter Halle et al. 2017). As the reaction proceeded, the available sites for oxidation on the surface of MPs gradually decreased, and the oxidation on the surface layer became saturated. In addition, the oxide layer on the surface would limit light penetration and oxygen diffusion into the interior of the MPs (Liu et al. 2019). Meanwhile, the PLA-MPs after 3 d irradiation with the coexistence of NDOM or BDOM presented nearly similar CI value (1.10 for NDOM, 1.14 for BDOM), which was about 1.2 times higher than that in pure water (0.93), and no obvious change was found for PLA-MPs in dark control. Compared to BDOM, NDOM took less time to reach the plateau stage, which suggested that NDOM might accelerate the photodegradation process more efficiently.

To further clarify the oxidation degree of photodegraded PLA-MPs, XPS analysis was conducted to examine their surface elemental compositions. The C1s spectra of pristine PLA-MPs and photodegraded PLA-MPs with NDOM and BDOM treatment were shown in Fig. 4. The main peaks at 284.6, 288.5 and 285.9 eV in C1s spectrum were assigned to C–C/C-H, O-C=O, and C-O band in pristine PLA-MPs, which accounted for 76.7%, 14.5% and 8.9%, respectively (Kiss et al. 2002). After 7 d irradiation, the content of C–C/C-H of PLA-MPs decreased to 71.0% and 66.7% under the influence of BDOM and NDOM, respectively. In addition, a new peak around 283.5 eV (corresponding to C–O–C) emerged in photodegraded PLA-MPs, suggesting the surface oxidation of PLA-MPs. This was also demonstrated in the FTIR analysis above. Thus, it was reasonable to speculate that parts of C–C/C-H ultimately were changed to C-O/C=O/O-C=O groups during the photodegradation. Besides, the O/C ratio calculated from the XPS result further validated this point. Similar to the FTIR result, Table S2 revealed that the O/C ratios of PLA-MPs in NDOM (0.71) and BDOM (0.58) after 7 d irradiation were greater than that of virgin PLA-MPs (0.43), indicating the higher oxygen content in photodegraded PLA-MPs. Especially, the O/C ratio of PLA-MPs in NDOM was higher than that in BDOM, suggesting that PLA-MPs in NDOM were more prone to be photodegraded than those in BDOM.

In addition to the oxidation of PLA-MPs, the chain scission was also important. ^{1}H-NMR, as an important technique to uncover the change of chemical structures of polymer, was applied to explore the change of chain structure during PLA-MPs photodegradation (Martín-Alfonso et al. 2019). As seen from Fig. S3 and Table S3, all samples after 7 d irradiation revealed a decrease of polymerization and molecular weight (Table S3). The

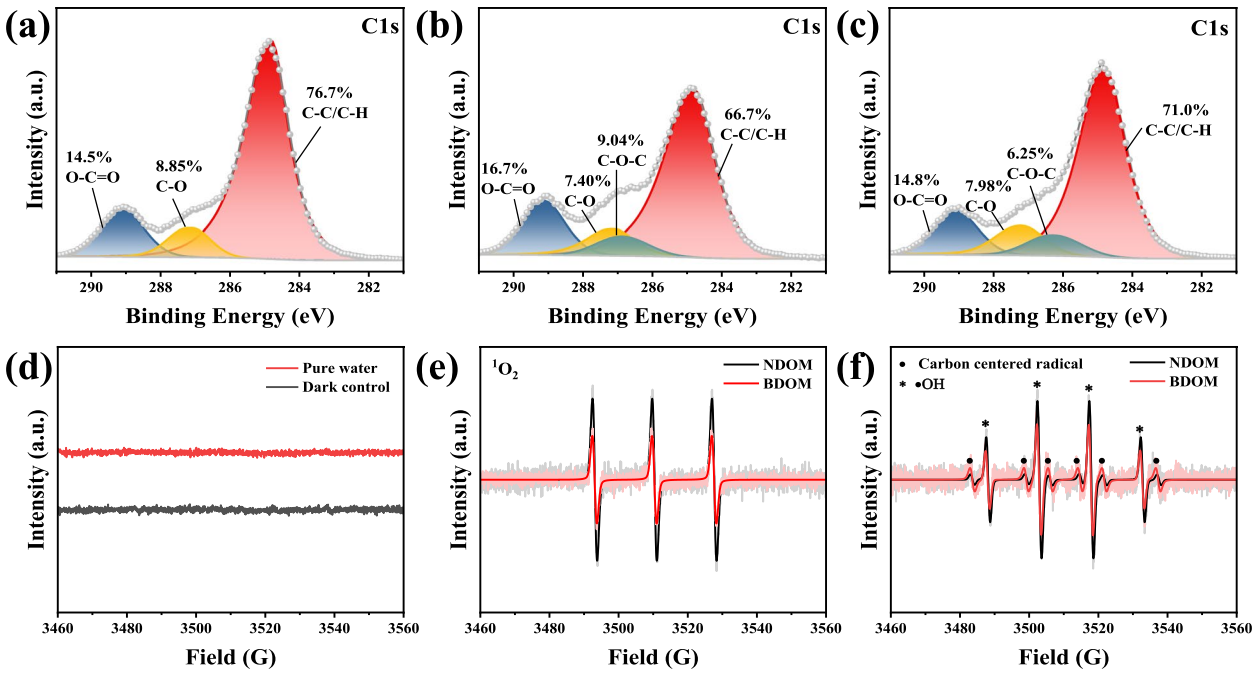

Fig. 4 X-ray photoelectron spectrums of photodegraded polylactic acid (PLA) microplastics (MPs) under 7 d irradiation in pure water (**a**), natural dissolved organic matter (NDOM) (**b**) and biochar-derived dissolved organic matter (BDOM) (**c**) solution; Electron paramagnetic resonance spectrums in dark control and pure water (**d**), the signal of $^{1}O_2$ (**e**), •OH and carbon-centered radial (**f**) in NDOM and BDOM solution under irradiation. Note that $^{1}O_2$ and •OH represented singlet oxygen and hydroxyl radicals, respectively

PLA-MPs subjected to NDOM treatment exhibited the lowest average degree of polymerization ($n = 27.5$) and molecular weight (MW = 2144), implying a more substantial depolymerization of PLA-MPs during photodegradation, resulting in the production of lower-molecular-weight species such as lactic acid monomers and oligomers. (Solarski et al. 2008).

3.3 Altered structures of BDOM and NDOM during photodegradation of PLA-MPs

As discussed above, the presence of BDOM and NDOM exhibited the eminent promoting effect on PLA-MPs photodegradation. Analyzing structural changes of BDOM and NDOM during the photodegradation process would help elucidate the roles of the two DOM in the process of PLA-MPs photodegradation. As shown in Fig. S4, the structures of BDOM and NDOM showed a regular variation pattern with prolonged reaction time. It was clear that the relative abundance of HA-like fractions of both NDOM and BDOM gradually decreased from 73.4% and 63.9% to 9.1% and 21.4%, respectively, in which the HA-like fraction decreased more significantly in NDOM than that in BDOM. Considering the more pronounced particle size reduction and higher carbonyl index of PLA-MPs in the presence of NDOM, it was suggested that the aromatic structures of NDOM were more likely to participate in the photodegradation of PLA-MPs compared to BDOM. Similarly, the $SUVA_{254}$ value of NDOM and BDOM showed decreasing trend with increasing time (Fig. S4a and b). Coupled with the ESI-FT-ICR-MS analysis, the higher AI in NDOM than that in BDOM indicates that more aromatic structures (e.g., condensed aromatic structures) in NDOM might contribute more to PLA-MPs photodegradation. Similar results were also found in the photodegradation system of pure DOM in another study (Zhang et al. 2020). It could be inferred that the chromophore involved in aromatic fractions of NDOM and BDOM could increase the light adsorption and accelerate the formation of $^3DOM^*$ during PLA-MPs photodegradation, as evidenced in previous research (Bianco et al. 2014; Wang et al. 2018). Furthermore, it was interesting that NDOM displayed a continuous downward trend in the content of HA-like components and aromaticity during 7 d irradiation, while for BDOM, the decreasing trend of HA-like abundance was gentle after 1 d (Fig. S4c). Moreover, it was observed that at the later period, the $SUVA_{254}$ value of BDOM was slightly increased, which might be partly ascribed to the preferential sorption of non-aromatic components by PLA-MPs as demonstrated below. At the end of the reaction, NDOM even showed lower aromaticity than BDOM, suggesting that more aromatic components of NDOM were converted.

3.4 The generated $^3DOM^*$ and ROS during photodegradation of PLA-MPs

To verify the role of aromatic components of NDOM and BDOM in the photoinduced transformation of PLA-MPs, the dominant free radical during the photodegradation process was monitored via EPR spectroscopy. As shown in Fig. 4d, no change was observed in EPR spectra for the dark control or pure water treatment, suggesting no obvious formation of radicals in dark condition or pure water. However, with the presence of NDOM and BDOM, carbon-centered radicals and ROS (•OH, $^1O_2$) were clearly detected. These radicals might induce the photodegradation of PLA-MPs such as the surface group transformation (C–C/C-H to C-O/C=O/O-C=O), as mentioned in the XPS analysis above. Additionally, it was noted that the signals of $^1O_2$ were different between NDOM and BDOM solution (Fig. 4e), which was derived from the reaction of $^3DOM^*$ and dissolved oxygen (Mcneill and Canonica 2016). Due to the high content of aromatic components in NDOM, it was supposed to produce more $^3DOM^*$ during light irradiation, leading to the enhanced $^1O_2$ formation. Meanwhile, the signal of carbon-centered radicals and the •OH was simultaneously found (Fig. 4f). Interestingly, compared to BDOM, the lower signal of carbon-centered radicals and the higher intensity of •OH were seen in the NDOM solution, indicating that more •OH formation was accompanied by the elimination of carbon-centered radicals. During the quenching experiment, it was noted that after quenching •OH, the size reduction of PLA-MPs dropped from 62.8% and 59.1% to 9.1% and 17.0% for NDOM and BDOM, respectively, further revealing the dominant role of •OH in PLA-MPs photodegradation compared to $^1O_2$ (28.1% for NDOM and 27.8% for BDOM after quenching) and $^3DOM^*$ (30.9% for NDOM and 33.9% for BDOM after quenching) (Fig. S5a). The production of •OH from DOM could occur via photo-generated H_2O_2 from DOM, or water oxidation by photochemically excited DOM (Berg et al. 2019). Due to the aromatic component in DOM as a major contributor to photoinduced $^3DOM^*$ (Liu et al. 2021), it was considered that the carbon-centered radicals may originate from $^3DOM^*$, followed by the combination with H of water to increase •OH generation. However, the mechanism of $^3DOM^*$ mediated •OH production was not clear. In the present study, a possible mechanism of $^3DOM^*$ mediating •OH generation was proposed: DOM was excited by light to generate $^3DOM^*$, followed by the stripping of the carbon-centered radical, which was bound to H in water, leading to the production of •OH. The quantification of different free radicals further revealed that the steady-state concentrations of •OH in NDOM solution were relatively high ($[•OH]_{ss} = 3.6 \times 10^{-12}$ M for NDOM and 2.5×10^{-12} M

for BDOM) compared to $^1O_2$ ($[^1O_2]_{ss} = 7.2 \times 10^{-13}$ M for NDOM and 1.6×10^{-13} M for BDOM) (Fig. S5b-d, Table S5). Considering the high abundance of aromatic components in NDOM fraction and the stronger promoting effect in PLA-MPs photodegradation, it could be inferred that the ROS generation was correlated with the aromatic constituents within DOM, to a great extent, and more •OH could be formed with more aromatic structures involved in NDOM solution. Additionally, more chromophores in the aromatic fraction could increase light adsorption. Berg et al. (2019) have found that DOM formulas with more aromatic components were most efficient at forming •OH, and Wang et al. (2018) have also confirmed that DOM contained a high percentage of aromatic fraction, which exhibited strong light absorption, resulting in the enhanced reactivity on photodegradation. Their finding could support our results that NDOM accelerated •OH generation since NDOM contained higher aromatic contents.

3.5 Mediating mechanisms of NDOM and BDOM in photodegradation of PLA-MPs

According to the analysis of $^3DOM^*$ and ROS, the aromatic components of two DOM occupied a significant role during the PLA-MPs photodegradation. The aromatic components of DOM might be excited in the solution or/and on the surface of PLA-MPs if they were preferentially sorbed by PLA-MPs. However, it was unclear which site (in the solution or sorbed on the surface of PLA-MPs) was dominant. To clarify the exciting site of the aromatic component and the possible mechanism, the sorption of NDOM and BDOM on PLA-MPs in dark control was conducted. Fig. S6a exhibited the sorption isotherms of NDOM and BDOM on PLA-MPs. Pseudo-first-order kinetic and pseudo-second-order kinetic equations were modeled, and the related kinetic parameters were obtained in Table S6. It can be seen that correlation coefficients (R^2) of the pseudo-second-order kinetic models for two DOM were higher than those of the pseudo-first-order kinetic, demonstrating that the sorption between PLA-MPs and DOM (NDOM and BDOM) was dominated by chemisorption (Sun et al. 2022). The sorption of PLA-MPs on NDOM reached the sorption equilibrium within 2 h, while the sorption on BDOM climbed the plateau within 24 h. Meanwhile, PLA-MPs exhibited a faster sorption rate for NDOM (0.280) relative to BDOM (0.002), indicating that PLA-MPs exhibited a stronger sorption affinity for NDOM. To further investigate which components of NDOM and BDOM were sorbed by PLA-MPs, EEM was applied to illustrate the alteration of components in the DOM solution before and after sorption. As shown in Fig. 1b and g**,** the intensity of the fluorescence peaks for both NDOM and BDOM decreased after sorption by PLA-MPs (Fig. 1c and h). Also, it was distinctly noted that after sorption, DOM remaining in the solution contained a higher abundance of fulvic acid- and humic acid-like species (Fig. 1j), and $SUVA_{254}$ value was enhanced from 2.9 and 1.2 to 3.4 and 1.6 for NDOM and BDOM, respectively (Fig. 1k), while the relative abundance of microbial by-product analogues reduced. Additionally, similar results were also seen from the FTIR analysis of BDOM or NDOM remaining in solution and PLA-MPs before and after sorption. As displayed in Fig. S7, for both BDOM and NDOM, the peak intensity at 2846 cm^{-1} and 2922 cm^{-1}, correlated to CH and CH_2 of aliphatic (Francioso et al. 2002), was obviously decreased after sorption. Meanwhile, the enhanced intensity was found for peaks at the same position of PLA-MPs after sorption, indicating the sorption of these nonaromatic components of NDOM and BDOM by PLA-MPs. In particular, this trend was more evident with the NDOM treatment. Additionally, the same change pattern was found in the peak at 1458 cm^{-1} and 1082 cm^{-1} (assigned to the aliphatic group) for NDOM. These analyses jointly suggested that PLA-MPs preferentially sorb microbial by-product analogue and aliphatics, leading to the aromatic components enriched in solution, and this preference was more evidently observed in the NDOM system. Thus, it could be concluded that the aromatic components of DOM were primarily excited in the solution. Moreover, the enriched aromatic components in solution due to the occurrence of preferential sorption of non-aromatics by PLA-MPs would help to accelerate the formation of $^3DOM^*$ in solution under irradiation, thereby promoting the photodegradation of PLA-MPs. For the preferentially sorbed non-aromatics, they would have a negligible blocking effect on light absorption of PLA-MPs due to their poor light-harvesting ability and relatively low content sorbed (Li et al. 2018b).

To further evaluate the light shielding effect of DOM sorbed onto the PLA-MPs, the light screening factor (S_λ) was calculated (Fig. S6b and c). As the reaction time prolonged, there was a slight increase for S_λ of the NDOM remained in the solution (aromatic fraction) and S_λ was generally unchanged for BDOM. The result reflected a weakened shielding effect for the remained fraction of DOM especially NDOM. This was ascribed to the enrichment of the aromatics in the solution, exhibiting more chromophores for light adsorption. For the photodegraded PLA-MPs, the S_λ hardly changed during the pure photolysis. Interestingly, after the addition of NDOM and BDOM, the S_λ showed basically the same trend as that of pure photolysis even though a small fluctuation was observed. Considering the small proportion of non-aromatic fraction (unsaturated hydrocarbons, lipids, and

carbohydrates, etc.) of the DOM composition (4.18% in NDOM and 3.43% in BDOM) (Fig. 1i), as well as the weak equilibrium adsorption capacity (q_e) of PLA-MPs (q_e = 2.19 mg/g for NDOM and 2.65 mg/g for BDOM) (Fig. S6a), it could be deduced that the shielding effect of the non-aromatic sorbed onto PLA-MPs was negligible. The quenching effect was also evaluated by calculating the quenching factor (Q_λ) (Xue et al. 2019). The value of S/S_λ (S: the observed light shielding factor) was found to be greater than 1, leading to the negative value of Q_λ (Table S7), and the ROS generated by DOM showed a stronger signal in the EPR plots (Fig. 4e and f), indicating that the quenching effect could be inconspicuous.

Based on the above results and discussions, the plausible mechanisms of DOM for accelerating the photodegradation of PLA-MPs were proposed in Fig. 5. Firstly, the DOM in the solution was excited under UV irradiation to generate $^3DOM^*$, in which the aromatic components played significant roles. The generated $^3DOM^*$ induced O_2 to form $^1O_2$ by energy transfer since it was well known as the precursor of $^1O_2$. On the other hand, $^3DOM^*$ oxidized water to generate •OH, which generated carbon-centered radicals, followed by the combination with H in water to produce •OH. The generated ROS (•OH and $^1O_2$) subsequently attacked the PLA-MPs, leading to the cracked morphology, reduced particle size, and increased oxygen-containing group on the surface. The depolymerization of PLA-MPs has been evidenced to follow the Norrish type II photoinduced cleavage (Ainali et al. 2022). As depicted in Fig. 5, DOM-induced •OH participated in the chain scission, especially by abstracting the H of C adjacent to C=O in PLA-MPs, which is involved in chain initiation and accelerates the degradation of PLA-MPs. Due to the abundant aromatic constituents contained in NDOM, more $^3DOM^*$ was produced, which promoted ROS (e.g., •OH) formation and accelerated the photodegradation of PLA-MPs. Also, this accelerating process was improved by the sorption of DOM by PLA-MPs. During the sorption, non-aromatic components were preferentially sorbed by PLA-MPs, resulting in the enrichment of aromatics in the solution and consequently, more $^3DOM^*$ was formed.

4 Conclusions

Natural/pyrogenic DOM and MPs commonly coexist in aquatic environments. However, the role of natural and pyrogenic DOM in the photochemical behavior of biodegradable MPs is rarely studied. In this work, we have detailed the process of photodegradation of PLA-MPs in freshwater with the presence of typical natural and pyrogenic DOM. Meanwhile, the evolution of two DOM during MPs photodegradation was also explored. Compared with BDOM, aromatic components are higher in NDOM and are inclined to be enriched in the solution during the sorption process onto PLA-MPs. Thus, with more $^3DOM^*$ and ROS formation in the solution, NDOM more strongly promotes the photodegradation of PLA-MPs, which provides the theoretical guidance of MPs photodegradation in coexistence with DOM in the aquatic environment, and improves the understanding of the photochemical activity of different sources of DOM. Additionally, considering that there is no agreement on the mechanism of $^3DOM^*$ induced •OH generation in previous researches, we have proposed a possible mechanism that carbon-centered radical derived from $^3DOM^*$ can deprive the H of water, contributing to •OH formation, potentially enriching the theories of radical transformation in the removal of environmental contaminant.

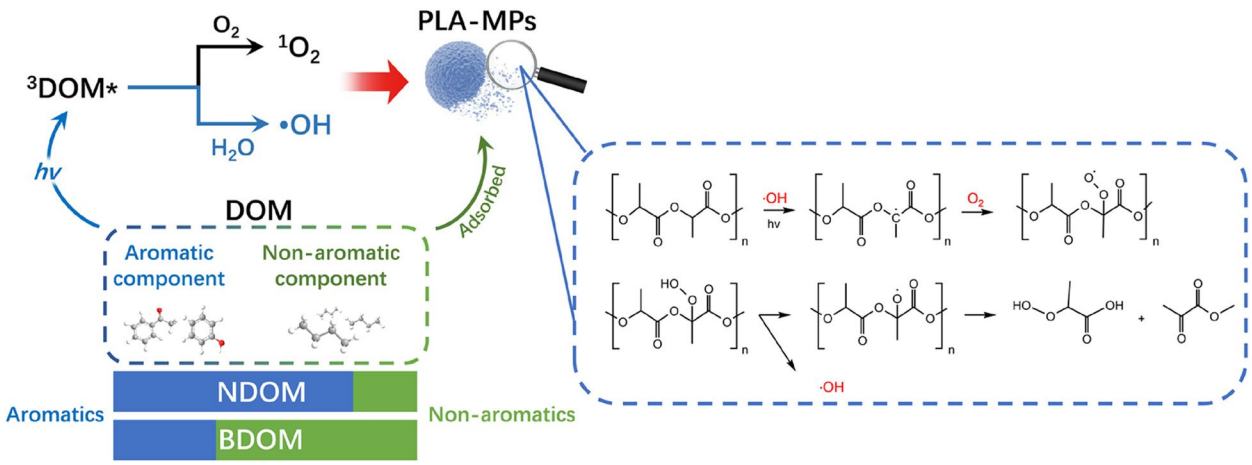

Fig. 5 The plausible mechanism of polylactic acid (PLA) microplastics (MPs) photodegradation in natural (NDOM) and biochar-derived dissolved organic matter (BDOM) solution. Note that $^1O_2$,•OH and $^3DOM^*$ represented singlet oxygen, hydroxyl radicals and the excited triplet states of DOM respectively

This work is anticipated to provide new insights into the photochemical transformation of biodegradable MPs which would potentially replace conventional MPs as the dominant MPs in environments in the future and help to differentiate the role of natural and pyrogenic DOM in this process. However, it should be noted that only one DOM concentration and one type of biodegradable MPs were investigated in this study, thus future works should be performed to include a range of DOM concentrations, various environmental factors (temperature, pH, salinity, etc.), different MP types (e.g., traditional microplastics and biodegradable microplastics) and concentrations to comprehensively unveil the process and mechanisms of MP photodegradation under more environmentally realistic conditions.

Supplementary Information

The online version contains supplementary material available at https://doi.org/10.1007/s44246-023-00050-8.

Additional file 1: Table S1. The magnitude-weighted averaged characteristics of NDOM and BDOM. **Table S2.** Variation of surface functional groups compositions and O/C of original and photodegraded polylactic acid (PLA)microplastics (MPs). **Table S3.** The number-average degree of polymerization (*n*) and number-average molecular weight (MW) of PLA from ^{1}H-NMR. **Table S4.** Trapping agents and reaction conditions of HPLC. **Table S5.** The qualification of different free radicals. **Table S6.** Kinetic parameters of natural and biochar-derived dissolved organicmatter sorption onto polylactic acid (PLA) microplastics (MPs). **Table S7.** The quenching effect analysis of dissolved organic matter (DOM). **Fig. S1.** Total organic carbon in the solution during photodegradation of polylactic acid (PLA) microplastics (MPs). **Fig. S2.** X-ray diffraction patterns of pristine and photodegraded polylactic acid (PLA) microplastics (MPs) in pure water (a), natural(NDOM) (b)and biochar-derived dissolved organic matter (BDOM) (c) solution after different time irradiation. **Fig. S3.** ^{1}H NMR spectra (600 MHz, $CDCl_3$) of pristine polylactide microplastics (PLA-MPs) (a) and those in pure water (b), biochar-derived (c) and natural dissolved organic matter (d) solution after 7 d irradiation. **Fig. S4.** Relative abundance from excitation-emission matrix spectrums of photodegraded polylacticacid (PLA) microplastics (MPs) in (a) natural and (b) biochar-derived dissolved organic matter solution under different time irradiation; aromaticity in the solution during PLA-MPs photodegradation (c). **Fig. S5.** Particle size reduction of polylactic acid(PLA) microplastics (MPs) after 3 d irradiation with different quencher addition in the presence of natural (NDOM) and biochar-derived dissolved organic matter (BDOM) (a); the qualification of ·OH (b) and $^{1}O_2$ (c).; the pseudo-first-order kinetics of FFA removal in the presence of $^{1}O_2$ (d). **Fig. S6.** The sorption plots of polylactic acid (PLA) microplastics (MPs) on natural (NDOM) and biochar-derived dissolved organic matter (BDOM) solution (a); the light screening factors (S_λ) of the fraction of NDOM and BDOM remaining in the solution (b) and sorbed onto the PLA-MPs during the photodegradation(c). **Fig. S7.** Fourier transform infrared (FTIR) spectraof polylactic acid (PLA) microplastics (MPs) (a) in different solution after sorption; FTIR of natural (NDOM) (b) and biochar-derived (c) dissolved organic matter (BDOM) before and after sorptionin dark condition.

Acknowledgements
The corresponding author thankfully acknowledge the financial support provided by the Program for Guangdong Introducing Innovative and Enterpreneurial Teams, National Natural Science Foundation of China and Young Elite Scientists Sponsorship Program by CAST. E.G.X. acknowledges the support of the Department of Biology, University of Southern Denmark, and Danmarks Frie Forskningsfond

Author's contributions
Jiehong He: Investigation, Data analysis, Writing—original draft; Weiwei Ma: Methodology, Investigation, Data analysis; Lanfang Han: Investigation, Experimental design, Correspondence, Funding acquisition, Writing—review & editing; Liying Chen: Investigation, Data analysis; Elvis Genbo Xu: Writing—review & editing; Baoshan Xing: Supervision, Writing—review & editing; Zhifeng Yang: Funding acquisition, Supervision, Writing—review & editing. The author(s) read and approved the final manuscript.

Funding
This word was supported by the Program for Guangdong Introducing Innovative and Enterpreneurial Teams (2019ZT08L213), National Natural Science Foundation of China (42277203), Young Elite Scientists Sponsorship Program by CAST (2021QNRC001). E.G.X. acknowledges the support of the Department of Biology, University of Southern Denmark, and Danmarks Frie Forskningsfond.
the Program for Guangdong Introducing Innovative and Enterpreneurial Teams,2019ZT08L213,National Natural Science Foundation of China,42277203,Lanfang Han,Young Elite Scientists Sponsorship Program by CAST,2021QNRC001

Availability of data and materials
The datasets used or analyzed during the current study are available from the corresponding author on reasonable request.

Declarations

Competing interest
The authors declare that they have no financial and non-financial competing interests.

Author details
[1]Key Laboratory for City Cluster Environmental Safety and Green Development of the Ministry of Education, School of Ecology, Environment and Resources, Guangdong University of Technology, Guangzhou 510006, China. [2]Southern Marine Science and Engineering Guangdong Laboratory (Guangzhou), Guangzhou 511458, China. [3]Department of Biology, University of Southern Denmark, 5230 Odense, Denmark. [4]School of Agriculture, University of Massachusetts, Amherst, MA 01003, USA.

Received: 21 February 2023 Revised: 1 April 2023 Accepted: 4 April 2023
Published online: 26 April 2023

References

Ainali NM et al (2022) Do poly(lactic acid) microplastics instigate a threat? A perception for their dynamic towards environmental pollution and toxicity. Sci Total Environ 832:155014
Ali MU, Lin S, Yousaf B, Abbas Q, Ming HW (2021) Environmental emission, fate and transformation of microplastics in biotic and abiotic compartments: Global status, recent advances and future perspectives. Sci Total Environ 791:135187
Berg SM et al (2019) The role of dissolved organic matter composition in determining photochemical reactivity at the molecular level. Environ Sci Technol 53(20):11725–11734
Bianco A et al (2014) Photochemical generation of photoactive compounds with fulvic-like and humic-like fluorescence in aqueous solution. Chemosphere 111:529–536
Buzarovska A, Gualandi C, Parrilli A, Scandola M (2015) Effect of TiO_2 nanoparticle loading on poly(l-lactic acid) porous scaffolds fabricated by TIPS. Compos B Eng 81:189–195
Canonica S (2007) Oxidation of aquatic organic contaminants induced by excited triplet states. Chimia 61(10):641–644
Chen C et al (2020) Impacts of microplastics on organotins' photodegradation in aquatic environments. Environ Pollut 267:115686
Chen C et al (2019) Organotin release from polyvinyl chloride microplastics and concurrent photodegradation in water: Impacts from salinity,

dissolved organic matter, and light exposure. Environ Sci Technol 53(18):10741–10752
Chen J, LeBoeuf EJ, Dai S, Gu B (2003) Fluorescence spectroscopic studies of natural organic matter fractions. Chemosphere 50(5):639–647
Ding L et al (2022a) Insight into interactions of polystyrene microplastics with different types and compositions of dissolved organic matter. Sci Total Environ 824:153883
Ding L et al (2022b) The photodegradation processes and mechanisms of polyvinyl chloride and polyethylene terephthalate microplastic in aquatic environments: Important role of clay minerals. Water Res 208:117879
Everaert G et al (2020) Risks of floating microplastic in the global ocean. Environ Pollut 267:115499
Filiciotto L, Rothenberg G (2021) Biodegradable plastics: Standards, policies, and impacts. Chemsuschem 14(1):56–72
Francioso O et al (2002) Spectroscopic study of humic acids fractionated by means of tangential ultrafiltration. J Mol Struct 609(1):137–147
Gao J, Liang C, Shen G, Lv J, Wu H (2017) Spectral characteristics of dissolved organic matter in various agricultural soils throughout China. Chemosphere 176:108–116
Gioia C et al (2021) End of life of biodegradable plastics: Composting versus re/upcycling. Chemsuschem 14(19):4167–4175
Goranov AI et al (2020) Photochemistry after fire: Structural transformations of pyrogenic dissolved organic matter elucidated by advanced analytical techniques. Geochim Cosmochim Acta 290:271–292
Hiemstra T, Mia S, Duhaut PB, Molleman B (2013) Natural and pyrogenic humic acids at goethite and natural oxide surfaces interacting with phosphate. Environ Sci Technol 47(16):9182–9189
Jaffé R et al (2013) Global charcoal mobilization from soils via dissolution and riverine transport to the oceans. Science 340(6130):345–347
Kalish JP, Aou K, Yang X, Hsu SL (2011) Spectroscopic and thermal analyses of α′ and α crystalline forms of poly(l-lactic acid). Polymer 52(3):814–821
Kim SW, Waldman WR, Kim TY, Rillig MC (2020) Effects of different microplastics on nematodes in the soil environment: tracking the extractable additives using an ecotoxicological approach. Environ Sci Technol 54(21):13868–13878
Kiss É, Bertóti I, Vargha-Butler EI (2002) XPS and wettability characterization of modified poly(lactic acid) and poly(lactic/glycolic acid) films. J Colloid Interface Sci 245(1):91–98
Leroy A et al (2017) FTIR microscopy contribution for comprehension of degradation mechanisms in PLA-based implantable medical devices. J Mater Sci-Mater m 28(6):87
Li J, Liu H, Chen JP (2018a) Microplastics in freshwater systems: A review on occurrence, environmental effects, and methods for microplastics detection. Water Res 137:362–374
Li Q, Tang Y, Hu W, Li Z (2018b) Fluorescence of nonaromatic organic systems and room temperature phosphorescence of organic luminogens: The intrinsic principle and recent progress. Small 14(38):1801560
Li Y, Wei X, Chen J, Xie H, Zhang YN (2015) Photodegradation mechanism of sulfonamides with excited triplet state dissolved organic matter: A case of sulfadiazine with 4-carboxybenzophenone as a proxy. J Hazard Mater 290:9–15
Liao J, Chen Q (2021) Biodegradable plastics in the air and soil environment: Low degradation rate and high microplastics formation. J Hazard Mater 418:126329
Lin Z et al (2022) Current progress on plastic/microplastic degradation: Fact influences and mechanism. Environ Pollut 304:119159
Liu H et al (2021) Humic acid extracts leading to the photochemical bromination of phenol in aqueous bromide solutions: Influences of aromatic components, polarity and photochemical activity. Molecules 26(3):608
Liu P et al (2022) Polystyrene microplastics accelerated photodegradation of co-existed polypropylene *via* photosensitization of polymer itself and released organic compounds. Water Res 214:118209
Liu P et al (2019) New insights into the aging behavior of microplastics accelerated by advanced oxidation processes. Environ Sci Technol 53(7):3579–3588
Luo H et al (2022) Interactions between polypropylene microplastics (PP-MPs) and humic acid influenced by aging of MPs. Water Res 222:118921
Luo Y et al (2021) Identification of sources, characteristics and photochemical transformations of dissolved organic matter with EEM-PARAFAC in the Wei River of China. Front Env Sci Eng 15(5):96
Lv J et al (2016) Molecular-scale investigation with ESI-FT-ICR-MS on fractionation of dissolved organic matter induced by adsorption on iron oxyhydroxides. Environ Sci Technol 50(5):2328–2336
Lv S, Gu J, Tan H, Zhang Y (2018) Enhanced durability of sustainable poly (lactic acid)-based composites with renewable starch and wood flour. J Clean Prod 203:328–339
Lyu L et al (2021) Characterization of dissolved organic matter (DOM) in an urbanized watershed using spectroscopic analysis. Chemosphere 277:130210
Mao R et al (2020) Aging mechanism of microplastics with UV irradiation and its effects on the adsorption of heavy metals. J Hazard Mater 393:122515
Martín-Alfonso JE, Urbano J, Cuadri AA, Franco JM (2019) The combined effect of H_2O_2 and light emitting diodes (LED) process assisted by TiO_2 on the photooxidation behaviour of PLA. Polym Test 73:268–275
Mcneill K, Canonica S (2016) Triplet state dissolved organic matter in aquatic photochemistry: Reaction mechanisms, substrate scope, and photophysical properties. Environ Sci-Proc Imp 18(11):1381
Miao Y, Lv J, Huang H, Cao D, Zhang S (2020) Molecular characterization of root exudates using Fourier transform ion cyclotron resonance mass spectrometry. J Environ Sci 98:22–30
Miranda MN, Sampaio MJ, Tavares PB, Silva AMT, Pereira MFR (2021) Aging assessment of microplastics (LDPE, PET and uPVC) under urban environment stressors. Sci Total Environ 796:148914
Niu XZ, Moore EG, Croue JP (2018) Excited triplet state interactions of fluoroquinolone norfloxacin with natural organic matter: A laser spectroscopy study. Environ Sci Technol 52(18):10426–10432
Pamuła E, Błażewicz M, Paluszkiewicz C, Dobrzyński P (2001) FTIR study of degradation products of aliphatic polyesters-carbon fibres composites. J Mol Struct 596(1):69–75
Paragkumar NT, Edith D, Six JL (2006) Surface characteristics of PLA and PLGA films. Appl Surf Sci 253(5):2758–2764
Qin M et al (2021) A review of biodegradable plastics to biodegradable microplastics: Another ecological threat to soil environments? J Clean Prod 312:127816
Qiu X et al (2022) Dissolved organic matter promotes the aging process of polystyrene microplastics under dark and ultraviolet light conditions: The crucial role of reactive oxygen species. Environ Sci Technol 56(14):10149–10160
Ryan CC, Tan DT, Arnold WA (2011) Direct and indirect photolysis of sulfamethoxazole and trimethoprim in wastewater treatment plant effluent. Water Res 45(3):1280–1286
Sang T, Wallis CJ, Hill G, Britovsek GJP (2020) Polyethylene terephthalate degradation under natural and accelerated weathering conditions. Eur Polym J 136:109873
Shi J et al (2016) Bioavailability of riverine dissolved organic carbon and nitrogen in the Heilongjiang watershed of northeastern China. Environ Monit Assess 188(2):113
Shi Y, Liu P, Wu X, Shi H, Gao S (2021) Insight into chain scission and release profiles from photodegradation of polycarbonate microplastics. Water Res 195(4):116980
Simmons H, Tiwary P, Colwell JE, Kontopoulou M (2019) Improvements in the crystallinity and mechanical properties of PLA by nucleation and annealing. Polym Degrad Stab 166:248–257
Solarski S, Ferreira M, Devaux E (2008) Ageing of polylactide and polylactide nanocomposite filaments. Polym Degrad Stab 93(3):707–713
Sun K et al (2016) Variation in sorption of propiconazole with biochars: The effect of temperature, mineral, molecular structure, and nano-porosity. Chemosphere 142:56–63
Sun Y, Wang X, Xia S, Zhao J (2022) Cu(II) adsorption on poly(lactic acid) microplastics: Significance of microbial colonization and degradation. Chem Eng J 429:132306
ter Halle A et al (2017) To what extent are microplastics from the open ocean weathered? Environ Pollut 227:167–174
Wagner S, Jaffé R, Stubbins A (2018) Dissolved black carbon in aquatic ecosystems. Limnol Oceanogr Lett 3(3):168–185
Wang C et al (2020) Photo-aging of polyvinyl chloride microplastic in the presence of natural organic acids. Water Res 183:116082

Wang C, Zhao J, Xing B (2021) Environmental source, fate, and toxicity of microplastics. J Hazard Mater 407:124357
Wang H, Lin HH, Hsieh M, Lin AY (2022) Photoaged polystyrene microplastics serve as photosensitizers that enhance cimetidine photolysis in an aqueous environment. Chemosphere 290:133352
Wang J et al (2018) DOM from mariculture ponds exhibits higher reactivity on photodegradation of sulfonamide antibiotics than from offshore seawaters. Water Res 144:365–372
Wang J, Chen J, Qiao X, Zhang Y, Uddin M (2019) Disparate effects of DOM extracted from coastal seawaters and freshwaters on photodegradation of 2,4-Dihydroxybenzophenone. Water Res 151:280–287
Wei X, Bohlén M, Lindblad C, Hedenqvist M, Hakonen A (2021) Microplastics generated from a biodegradable plastic in freshwater and seawater. Water Res 198:117123
Wei X et al (2022) Millions of microplastics released from a biodegradable polymer during biodegradation/enzymatic hydrolysis. Water Res 211:118068
Wen Z et al (2018) Differences in the distribution and optical properties of DOM between fresh and saline lakes in a semi-arid area of Northern China. Aquat Sci 80(2):22
Xiang Y et al (2022) Microplastics and environmental pollutants: key interaction and toxicology in aquatic and soil environments. J Hazard Mater 422:126843
Xue S et al (2019) Effect of dissolved organic matter fractions on photodegradation of phenanthrene in ice. J Hazard Mater 361:30–36
Yang S, Wu Z, Yang W, Yang M (2008) Thermal and mechanical properties of chemical crosslinked polylactide (PLA). Polym Test 27(8):957–963
Yang Y et al (2022) Biochar stability and impact on soil organic carbon mineralization depend on biochar processing, aging and soil clay content. Soil Biol Biochem 169:108657
Zhang D, Yan S, Song W (2014) Photochemically induced formation of reactive oxygen species (ROS) from effluent organic matter. Environ Sci Technol 48:21
Zhang P, Shao Y, Xu X, Huang P, Sun H (2020) Phototransformation of biochar-derived dissolved organic matter and the effects on photodegradation of imidacloprid in aqueous solution under ultraviolet light. Sci Total Environ 724:137913
Zhu K et al (2020) Long-term phototransformation of microplastics under simulated sunlight irradiation in aquatic environments: Roles of reactive oxygen species. Water Res 173:115564
Zhu K et al (2019) Formation of environmentally persistent free radicals on microplastics under light irradiation. Environ Sci Technol 53(14):8177–8186

Publisher's Note